Developmental Cell *10*, 209–222, February, 2006 ©2006 Elsevier Inc. DOI 10.1016/j.devcel.2005.11.016

Polarized Transport of Frizzled along the Planar Microtubule Arrays in *Drosophila* Wing Epithelium

Yuko Shimada,[1] Shigenobu Yonemura,[2] Hiroyuki Ohkura,[3] David Strutt,[4] and Tadashi Uemura[1,5,*]

[1] Laboratory of Cell Recognition and Pattern Formation
Graduate School of Biostudies
South Campus Research Building (Building G), Room 118
Kyoto University
Yoshida Konoe-cho, Sakyo-ku
Kyoto 606-8501
Japan

[2] RIKEN Center for Developmental Biology
2-2-3 Minatojima-Minamimachi Chuo-ku
Kobe 650-0047
Japan

[3] Wellcome Trust Centre for Cell Biology
Institute of Cell Biology
School of Biological Sciences
The University of Edinburgh
Mayfield Road
Edinburgh EH9 3JR
United Kingdom

[4] Center for Developmental and Biomedical Genetics
Department of Biomedical Science
University of Sheffield
Western Bank
Sheffield S10 2TN
United Kingdom

[5] Core Research for Evolutional Science and Technology (CREST)
Japan Science and Technology Agency
Kawaguchi, Saitama 332-0012
Japan

Summary

Cells in a variety of developmental contexts sense extracellular cues that are given locally on their surfaces, and subsequently amplify the initial signal to achieve cell polarization. *Drosophila* wing cells acquire planar polarity along the proximal-distal (P-D) axis, in which the amplification of the presumptive cue involves assembly of a multiprotein complex that spans distal and proximal boundaries of adjacent cells. Here we pursue the mechanisms that place one of the components, Frizzled (Fz), at the distal side. Intracellular particles of GFP-tagged Fz moved preferentially toward distal boundaries before Fz::GFP and other components were tightly localized at the P/D cortex. Arrays of microtubules (MTs) were approximately oriented along the P-D axis and these MTs contributed to the formation of the cortical complex. Furthermore, there appeared to be a bias in the P-D MTs, with slightly more plus ends oriented distally. The hypothesis of polarized vesicular trafficking of Fz is discussed.

*Correspondence: tauemura@lif.kyoto-u.ac.jp

Introduction

Many classes of epithelial cells generate asymmetry not only along the apical-basal axis, but also along a second axis within a plane. This cell asymmetry along the planar axis, known as planar cell polarity (PCP) or tissue polarity, is remarkably coordinated and can be readily recognized by landmarks exposed on the epithelial surfaces, such as unidirectionally beating cilia in the respiratory epithelium and epidermal cuticular structures in insects including *Drosophila* (Lawrence, 1966). Each epidermal cell of the *Drosophila* wing assembles actin bundles at its distalmost vertex, producing a single prehair that extends away from the cell and thus acquiring proximal-distal (P-D) polarity (Figures 1A and 1B).

Numerous polarity mutants of *Drosophila* have been isolated and their gene products controlling PCP signaling subsequently identified (Adler, 2002; Eaton, 2003; Strutt, 2003). On the basis of mostly genetic studies, PCP proteins fall into two classes, and this classification fits into the general framework for discussing cell polarity, as follows. (1) A cassette of transmembrane proteins is involved in providing an extrinsic spatial cue on the cell surface to instruct orientation of the axis. (2) Receptors and downstream components interpret the cue and reinforce the asymmetry defined by the cue (Drubin, 2000).

Molecules of the second class include the founding member of the PCP signaling pathway Frizzled (Fz; Vinson et al., 1989), a seven-pass transmembrane cadherin, Flamingo/Starry night (Fmi/Stan; Chae et al., 1999; Usui et al., 1999), and the intracellular multimodular protein Dishevelled (Dsh; Klingensmith et al., 1994; Theisen et al., 1994). All of them are distributed at proximal and/or distal cell cortexes (Figure 1D) (Axelrod, 2001; Bastock et al., 2003; Feiguin et al., 2001; Katanaev et al., 2005; Shimada et al., 2001; Strutt, 2001; Tree et al., 2002; Usui et al., 1999). These proteins are proposed to form a multiprotein complex across the P/D boundary and are designated as the cortical domain proteins of the PCP pathway hereafter. This multiprotein complex is considered to serve as a feedback loop to amplify a small imbalance of Fz activity that is imparted by the upstream cassette, and eventually leads to restriction of the site of prehair formation at the distal cell end (Klein and Mlodzik, 2005; Lawrence et al., 2004; Strutt, 2002; Uemura and Shimada, 2003). One line of evidence underlying this model is that a wing cell, when a function of any one of the cortical domain proteins is lost, produces a prehair near the cell center (Figure 1C) (Wong and Adler, 1993). Evolutionally conserved cortical domain proteins play important roles in at least two polarized behaviors of vertebrate cells: sensory hair morphogenesis in the inner ear epithelium and convergent extension movements during gastrulation (Curtin et al., 2003; Mlodzik, 2002; Strutt, 2003; Torban et al., 2004; Veeman et al., 2003).

The following observations are consistent with the hypothesis that proximal and/or distal localization of the cortical domain proteins is a prerequisite for specifying

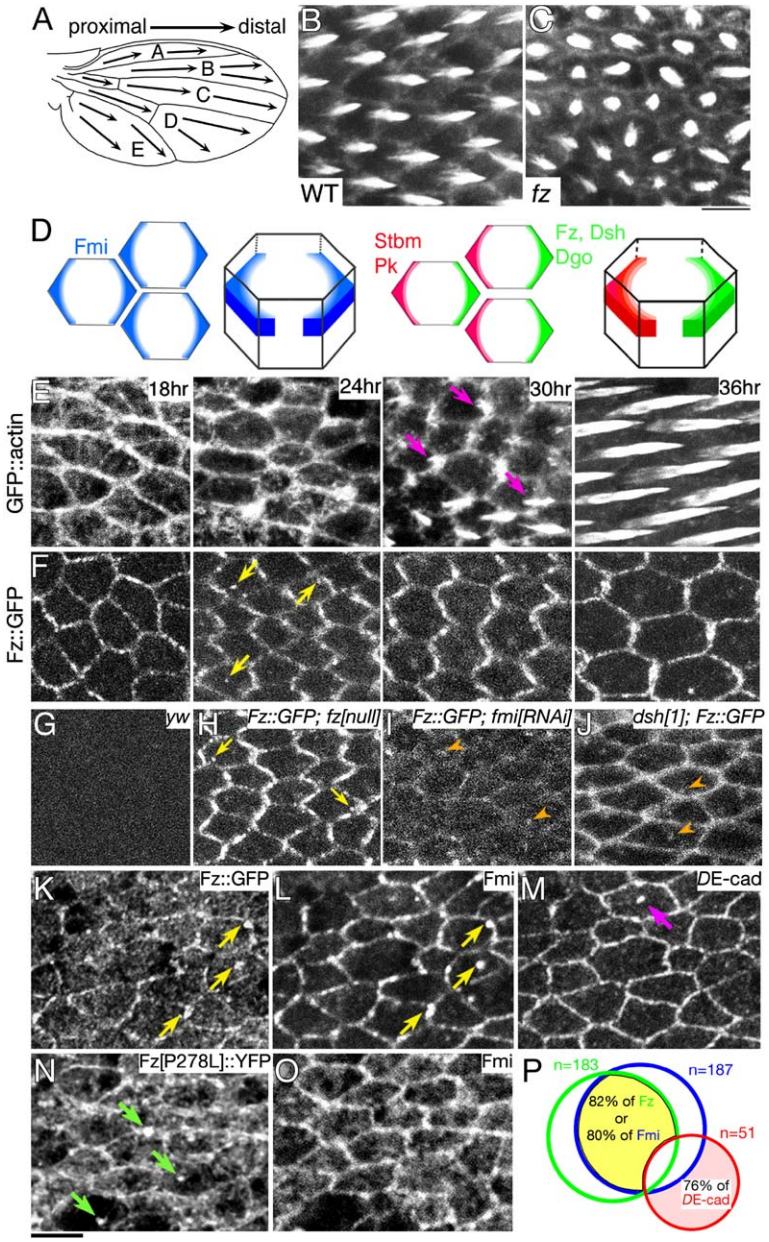

Figure 1. In Vivo Time-Lapse Imaging and Colocalization of Intracellular Frizzled::GFP Particles with Fmi

(A) A schema of the adult wing. In this and all subsequent figures, distal is to the right and anterior is at the top. At the level of individual cells, the P-D axis shifts slightly depending on where each cell is located within the wing, as indicated by arrows.

(B and C) Prehair formation visualized by GFP::actin on the wild-type (B) or *fz* null mutant (C) background.

(D) Localization of polarity regulators prior to the onset of prehair formation.

(E and F) Temporal dynamics of GFP::actin (E) and Fz::GFP (F) after puparium formation (APF). The sign of the distal localization is detected at 24 hr APF (note also bright intracellular particles indicated by yellow arrows), and the "zigzag" pattern becomes most prominent at 30 hr APF at the very onset of prehair formation (magenta arrows). Fz::GFP distribution becomes depolarized at 36 hr APF.

(G–J) Images of live 24 hr APF wings: cells that did not have the *Fz::GFP* transgene (G); Fz::GFP signals at both cell boundaries and inside cells (arrows) on the *fz* null mutant background (H); and blurry signals in dsh^{1} and fmi^{RNAi} mutant cells (arrowheads in [I] and [J], respectively).

(K–O) Triple stainings of 24 hr APF wings for Fz::GFP (K) or Fz^{P278L}::YFP (N), Fmi (L and O), and *D*E-cadherin (M). Fz::GFP particles containing Fmi (yellow arrows), *D*E-cadherin particles (magenta arrow), and Fz^{P278L}::YFP particles (green arrows) are highlighted.

(P) Venn diagram of Fz::GFP, Fmi, and *D*E-cadherin particles. Numbers of particles examined are indicated.

Genotypes were *en-GAL4/UAS-GFP::actin* (B and E), *en-GAL4/UAS-GFP::actin;* fz^{K21}/$Df(3L)fz^{D21}$ (C), *arm-Fz::GFP* (F and K–M), *yw* (G), *arm-Fz::GFP;* fz^{K21}/$Df(3L)fz^{D21}$ (H), *arm-Fz::GFP; da-GAL4/UAS-fmi dsRNA* (I), dsh^{1}/*Y; arm-Fz::GFP* (J), and *Act-*Fz^{P278L}*::YFP* (N and O). The scale bar represents 5 μm.

the hair formation site. (1) The molecules are localized at the cortexes only transiently before prehair formation. Once prehairs start growing, the distributions become depolarized (Strutt, 2001; Usui et al., 1999). (2) The cortical localization is highly cooperative in that elimination of any one of the proteins interferes with the polarization of all the others. (3) Ectopic distributions at anterior/posterior cortexes are correlated with prehair outgrowth at the anterior/posterior cell edges. (4) PCP is disrupted by overexpression of any one of the proteins (2–4: Axelrod, 2001; Bastock et al., 2003; Feiguin et al., 2001; Katanaev et al., 2005; Shimada et al., 2001; Strutt, 2001; Tree et al., 2002; Usui et al., 1999). (5) A chick homolog of Fmi shows a polarized distribution in each hair cell as Fmi does in the fly wing (Davies et al., 2005).

In spite of the potential importance of these asymmetrical distributions, the cell biological mechanism employed to localize the cortical domain proteins is a mystery (Adler, 2002; Eaton, 2003; Strutt, 2002, 2003), and this is the question that we attempted to solve. Three mechanisms for Fz localization that are not mutually exclusive are as follows: polarized vesicular transport, selective anchoring and retention at the distal boundary, and directional translocation within the plasma membrane (see Figure S1A in the Supplemental Data available with this article online). With these possibilities in mind, we performed in vivo time-lapse imaging of green fluorescent protein (GFP)-tagged Fz and also ultrastructural analysis of pupal wing cells with the primary focus on horizontal sections, where the multiprotein complex assembles. Our results highlighted the polarized vesicular transport hypothesis; that is, Fmi- and Fz::GFP-containing vesicles appear to be transported preferentially toward the distal cell cortex along microtubules (MTs) that are approximately oriented along the P-D axis. Furthermore, time-lapse recordings of an MT plus end

marker, EB1::GFP, showed that plus end-distal MTs were slightly more abundant than plus end-proximal MTs. This finding implies the possibility that the origin of the polarized vesicular trafficking could be traced back to asymmetry of the polarity of individual MTs.

Results

In Vivo Time-Lapse Imaging of Pupal Wing Cells

For monitoring GFP-tagged proteins, we established a protocol of in vivo time-lapse imaging of pupal wing cells (see details in Experimental Procedures and Figure S1B). Under the experimental conditions employed, about 90% of pupae eclosed, and wing development proceeded in terms of prehair formation and hair growth. Our time-lapse recordings revealed that GFP::actin in the wild-type wing cells underwent repeated cycles of assembly and disassembly at multiple sites of the cell periphery, until prehairs eventually emerged at distal cell ends (Figures 1B and 1E; Movie S1). Furthermore, we could monitor prehair formation at the center of the apical surface in *fz* mutant cells (Figure 1C; Movie S2) as previously reported to occur in fixed cells (Wong and Adler, 1993). These observations indicate that our protocol perturbed neither normal development nor manifestation of the *fz* phenotype.

Intracellular Fz::GFP Particles Are Present at the Level of Adherens Junction and Contain Fmi and Dsh, but Not *D*E-Cadherin

We observed GFP-tagged Fz that was expressed under the control of the *armadillo* promoter in living pupae (Strutt, 2001). It has been shown that this Fz::GFP expression rescues the *fz* loss-of-function phenotype and that the transgene expression on the wild-type background does not result in a gain-of-function phenotype, suggesting the total level of endogenous Fz plus transgenic Fz::GFP stays within the physiological range. Therefore, we expected that behaviors of Fz::GFP were functionally relevant to those of endogenous Fz. Under our imaging conditions for Fz::GFP, cells without the transgene gave essentially no signal (Figure 1G), and Fz::GFP-expressing cells displayed signals at intercellular boundaries and inside cells whether they produced endogenous Fz or not (Figures 1F and 1H). These results suggest that signals at both subcellular compartments represented those of Fz::GFP molecules, and so we designated the intracellular signals as Fz::GFP particles. Along the apicobasal axis, Fz::GFP particles were detected at the level of adherens junction (AJ), where cortical domain components of the PCP signaling pathway, such as Fmi and Dsh, are localized (Figure 1D; Figure S1C) (Axelrod, 2001; Shimada et al., 2001; Strutt, 2001; Usui et al., 1999). We hypothesize that these particles represent delivery of Fz::GFP to distal cell boundaries.

Fz::GFP particles were also observed in fixed tissues by staining with anti-GFP antibody (Figure 1K), and most likely these particles were equivalent to those detected in living animals. About 80% of Fz::GFP intracellular particles contained Fmi and vice versa (yellow arrows in Figures 1K and 1L; Figure 1P); in contrast, less than 7% of Fz::GFP or Fmi molecules were associated with *D*E-cadherin, the major adhesion molecule at AJ (magenta arrow in Figures 1M and 1P). Fz::GFP particles also contained Dsh (data not shown). As shown below, our immuno-EM analysis strongly suggested that Fz::GFP particles were vesicles; thus, these results favored the idea that the polarity regulators and *D*E-cadherin were sorted into distinct vesicles.

Fmi- and Dsh-Dependent Appearance of Fz::GFP Particles

Previous observations on fixed cells demonstrated that the P/D cell boundary distributions of the PCP regulators such as Fz::GFP and Fmi are interdependent (Axelrod, 2001; Bastock et al., 2003; Feiguin et al., 2001; Katanaev et al., 2005; Shimada et al., 2001; Strutt, 2001; Tree et al., 2002; Usui et al., 1999). We confirmed this mutual dependency in live cells (Figures 1I and 1J). Fz::GFP signals were greatly reduced at any cell boundaries when *fmi* expression was knocked down (Figure 1I), and Fz::GFP distribution was no longer restricted to distal boundaries when the polarity function of Dsh or Prickle (Pk) was impaired (Figure 1J; data of a *pk* mutant not shown). In addition to the distal boundary localization, the presence of bright Fz::GFP intracellular particles was also dependent on Fmi, Dsh, and Pk. Such particles were hardly seen in fmi^{RNAi}, dsh^{1}, or $pk^{pk\text{-}sple13}$ cells; instead, only blurry blobs were found (compare yellow arrows in Figure 1H with orange arrowheads in Figures 1I and 1J).

Because Fmi and Dsh mediate Fz signaling in a cell-autonomous fashion, we predicted that the existence of Fz::GFP particles might depend on the autonomous function of Fz. This prediction was verified by studying Fz^{P278L} which has an amino acid substitution in the first intracellular loop and retains its non-cell-autonomous function, but not the cell-autonomous one (Jones et al., 1996; Strutt, 2001). Fz^{P278L}::YFP was mislocalized at all cell/cell boundaries (Figure 1N) as shown previously (Strutt, 2001). Although particle signals of Fz^{P278L}::YFP were found more frequently than those of Fz::GFP, they hardly contained Fmi (5%, n = 340; arrows in Figures 1N and 1O).

Fz::GFP Particles Move Preferentially to Distal, Rather Than Proximal, Cell Boundaries prior to Prehair Formation

We tracked the movements of Fz::GFP particles at various time intervals. In our initial attempts, we took images of single optical sections every 1 or 10 s to make sure that we were tracking identical particles, and found that the particles showed staggered trajectories (Figure S2). Then we took serial images of optical sections along the Z axis to track particles in three dimensions and prolonged the interval up to 1 min to track behaviors of the particles for a longer time. Although the fluorescence of Fz::GFP was readily quenched, possibly due to the low-level expression, this recording allowed us to find that many particles moved in defined directions and reached cell boundaries (Figures 2A–2D). Figures 2A and 2B show that particles were moving distally and reached distal boundaries (see also Movies S3 and S4), whereas Figure 2C depicts a particle coming out of the distal boundary and then going back to the same one (Movie S5). When in contact with the boundary, the particle-shaped fluorescence appeared to be transformed into a short bar, possibly reflecting

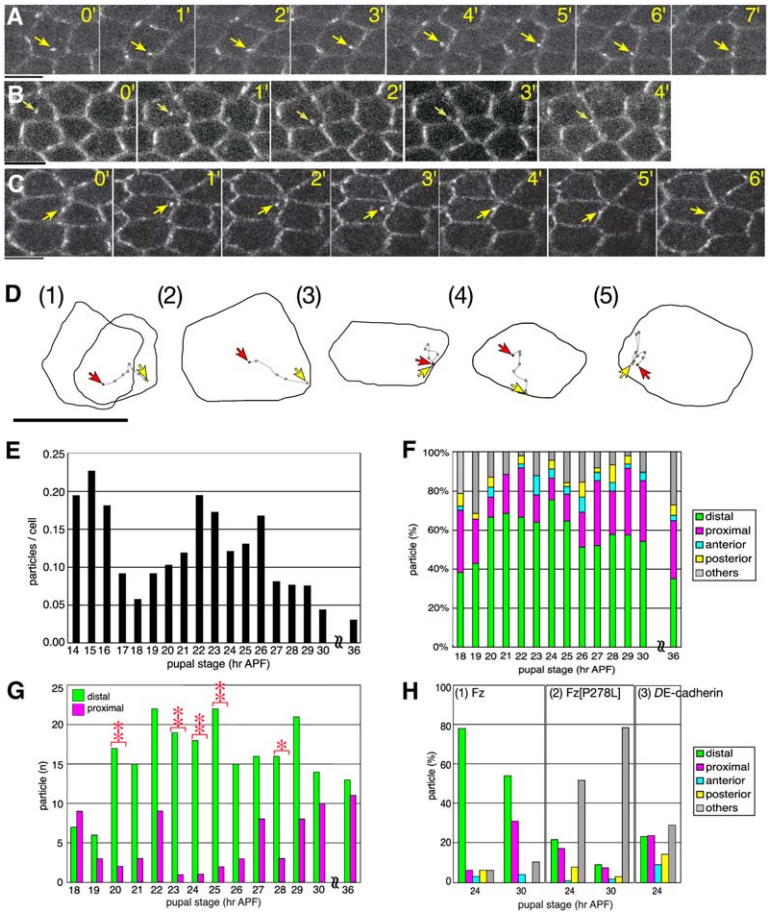

Figure 2. Fz::GFP Particles Moved to Preferentially Distal Cell Boundaries prior to Prehair Formation

(A–D and F–H) In vivo time-lapse analysis at 1 min intervals.

(A–C) Fz::GFP particles are indicated by yellow arrows.

(D) Examples of trajectories of Fz::GFP particles. Starting points and goals are indicated by red and yellow arrows, respectively. The scale bar represents 5 μm.

(E) The number of Fz::GFP particles at each pupal age. At each time point, Fz::GFP particles in 500–1000 cells, except for those in vein cells, were counted.

(F) Ratios of particles that moved toward the indicated cell boundaries at each pupal age. The gray box represents the ratio of particles that did not move in a specific direction before they were quenched. The number of particles examined at each age was 30–50.

(G) The number of particles that reached distal boundaries and the number of those that reached proximal ones were compared at each age (*$p < 0.005$ and **$p < 0.001$; binomial test).

(H) In contrast to Fz::GFP (1), Fz^{P278L}::YFP (2) and *D*E-cadherin::GFP (3) particles did not exhibit directional bias along the P-D axis at 24 or 30 hr APF.

incorporation of Fz::GFP into the plasma membrane domain (frame 6′ of Figure 2C).

Tracking individual Fz::GFP particles at different pupal ages provided two lines of evidence that were suggestive of a possible role of the particles in localizing Fz::GFP at distal boundaries. First, although the number of particles per cell fluctuated during pupal development, the value became locally maximal between 22 and 26 hr after puparium formation (APF), that is, 4–8 hr before the onset of prehair formation, whereas it was minimal at 36 hr APF when prehairs were growing (Figure 2E). Second, and more importantly, between 20 and 30 hr APF, about 60% of the particles moved along the P-D axis (Figure 2F). When we focused on particles that reached P/D cell boundaries during our recordings, the number of particles that reached distal boundaries far exceeded that of proximal boundary-arriving particles with statistical significance (asterisk and double asterisks in Figure 2G). The orientation of Fz::GFP particle movements was no longer biased toward distal boundaries at 30 hr APF, when the "zigzag" distribution characteristic of tight restriction to distal cell boundaries became most prominent.

The predominantly distal movement required the cell-autonomous function of Fz, and it was probably not a general feature of transmembrane proteins in pupal wing cells. This was shown by tracking intracellular particles of Fz^{P278L}::YFP and GFP-tagged *D*E-cadherin (Figure 2H). *D*E-cadherin::GFP is a functional adhesion molecule that can rescue loss-of-function phenotypes (Oda and Tsukita, 2001). In contrast to Fz::GFP, neither Fz^{P278L}::YFP nor *D*E-cadherin::GFP particles displayed preferentially distal tracks at 24 or 30 hr APF. Furthermore, Fz^{P278L}::YFP and *D*E-cadherin::GFP particles behaved differently from Fz::GFP particles in other respects. A majority of Fz^{P278L}::YFP particles displayed much less consistent paths compared with Fz::GFP particles and became undetectable before reaching any boundaries. "Blurry blobs" of Fz::GFP signals in fmi^{RNAi} or dsh^{1} cells (orange arrowheads in Figures 1I and 1J) showed similar behaviors (data not shown). *D*E-cadherin::GFP particles appeared to move faster than Fz::GFP particles, consistent with the hypothesis that *D*E-cadherin may be sorted into vesicles different from those containing Fz::GFP.

Individual Microtubules Are Visualized at the Level of Adherens Junction on Horizontal Sections

To study cellular machineries underlying the polar movement of Fz::GFP particles, we performed ultrastructural analysis of pupal wing cells. Because Fz::GFP particles moved at the level of AJ (arrows in Figure 3A), we prepared horizontal sections cut approximately parallel to the surface of epithelial layers and observed them by transmission electron microscopy (TEM) with a focus on the plane containing AJ (AJ plane in Figure 3B). AJ, which has an actin-rich undercoat, was recognized as electron-dense intercellular boundaries

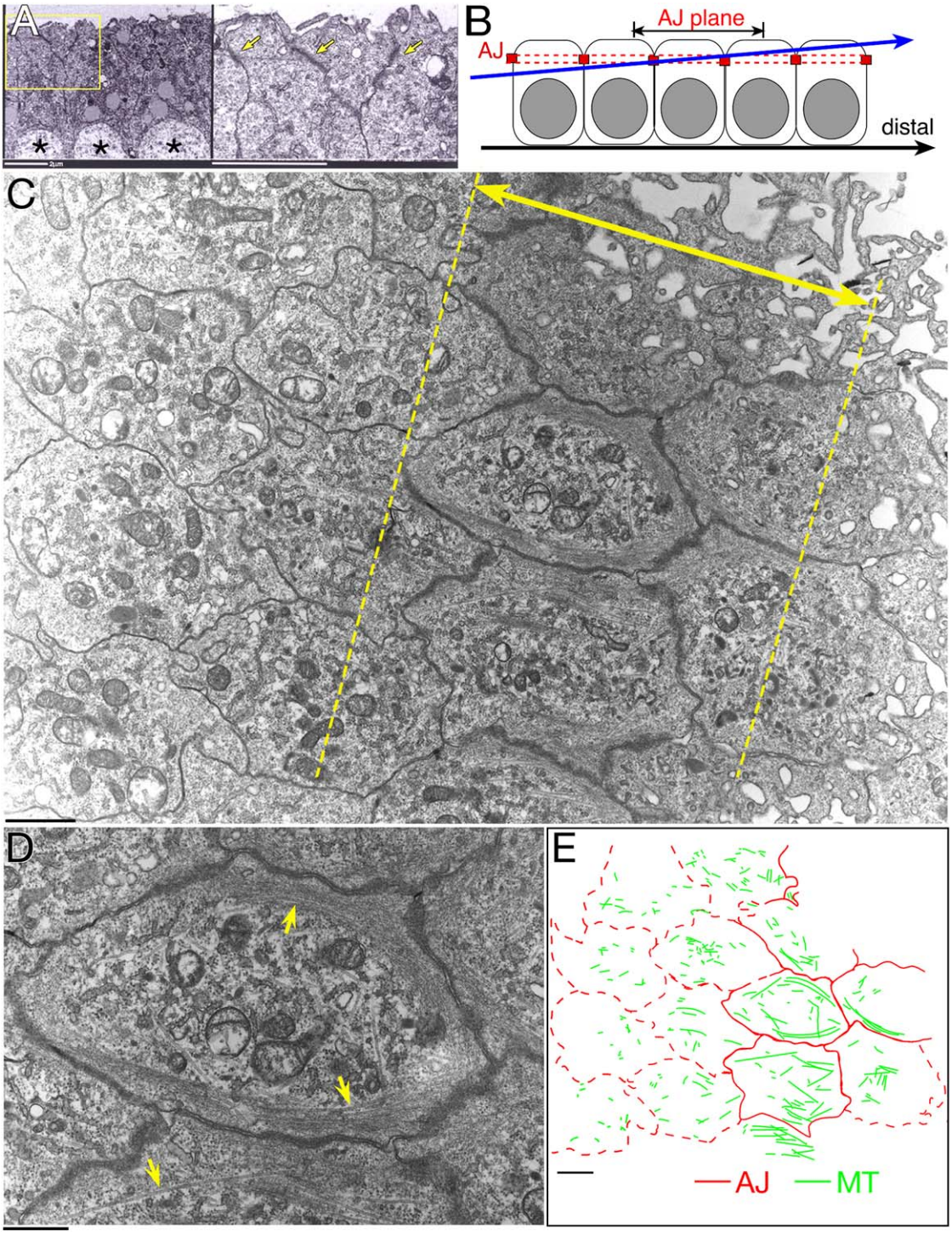

Figure 3. Visualization of Individual Microtubules on Horizontal Sections

(A) A vertical section of a pupal wing at 30 hr APF. Asterisks indicate nuclei. A high-power image of the boxed area is shown in the right panel. Electron-dense domains (yellow arrows) correspond to adherens junction (AJ).

(B–E) A schema of the cross-section (B) and horizontal sections (C–E) of 30 hr APF wings.

(C) The double-headed yellow arrow and broken lines demarcate the plane containing AJ (AJ plane in [B]) that was recognized on the basis of actin filament-rich undercoats along cell boundaries. This wing was cut at a small oblique angle with respect to the surface of the epidermal layer (blue line in [B]).

(D) A high-power image of (C); arrows indicate microtubules (MTs).

(E) Individual MTs and cell boundaries containing AJ are traced with green and red solid lines, respectively. Cell boundaries outside the AJ plane are traced with red broken lines. The scale bars represent 2 μm (A), 1 μm (C and E), and 500 nm (D).

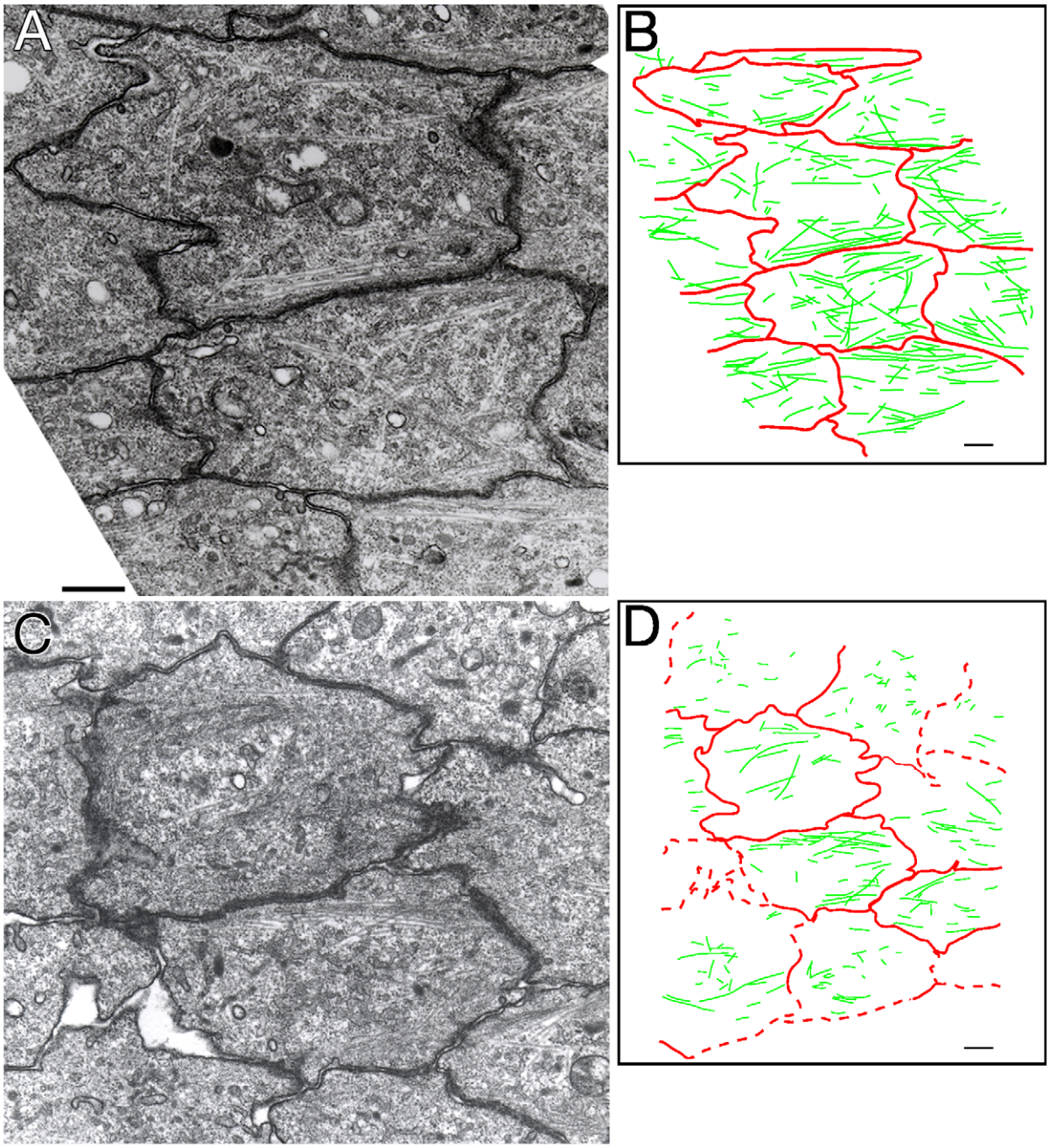

Figure 4. Microtubules at the AJ Level Were Preferentially Oriented along the P-D Axis

EM images of AJ planes at 24 hr APF (A and C) and tracings of MTs (green lines) and AJ (red solid lines) as in Figure 3E (B and D). The scale bar represents 500 nm.

on the sections (double-headed arrow in Figure 3C). At both 24 and 30 hr APF, the AJ plane was rich in MTs, which were identified on the basis of their diameter (25–30 nm); in contrast, such planar MTs were much less abundant at other levels (Figures 3C–3E and 4A–4D). This result is consistent with the "apical MT web" reported to exist in pupal wings from staining experiments for tubulin and EM images of cross-sections of imaginal discs (Eaton et al., 1996; Fristrom and Fristrom, 1975; Turner and Adler, 1998). Hereafter, we designate MTs on the AJ plane as apical MTs. In contrast to 24 or 30 hr APF, MTs were hardly found at 36 hr APF, when prehairs had already emerged and Fz::GFP distribution was no longer restricted to distal cell boundaries (Figure S3).

Microtubules on the AJ Plane Are Preferentially Oriented along the P-D Axis of the Wing

On the AJ plane, numerous MTs pointed toward proximal and distal cell boundaries either along cell borders or inside cells; in contrast, few MTs ran toward anterior and posterior cell boundaries, almost perpendicular to the P-D axis (Figures 3D, 3E, and 4A–4D). For graphic representation of the MT organization in terms of

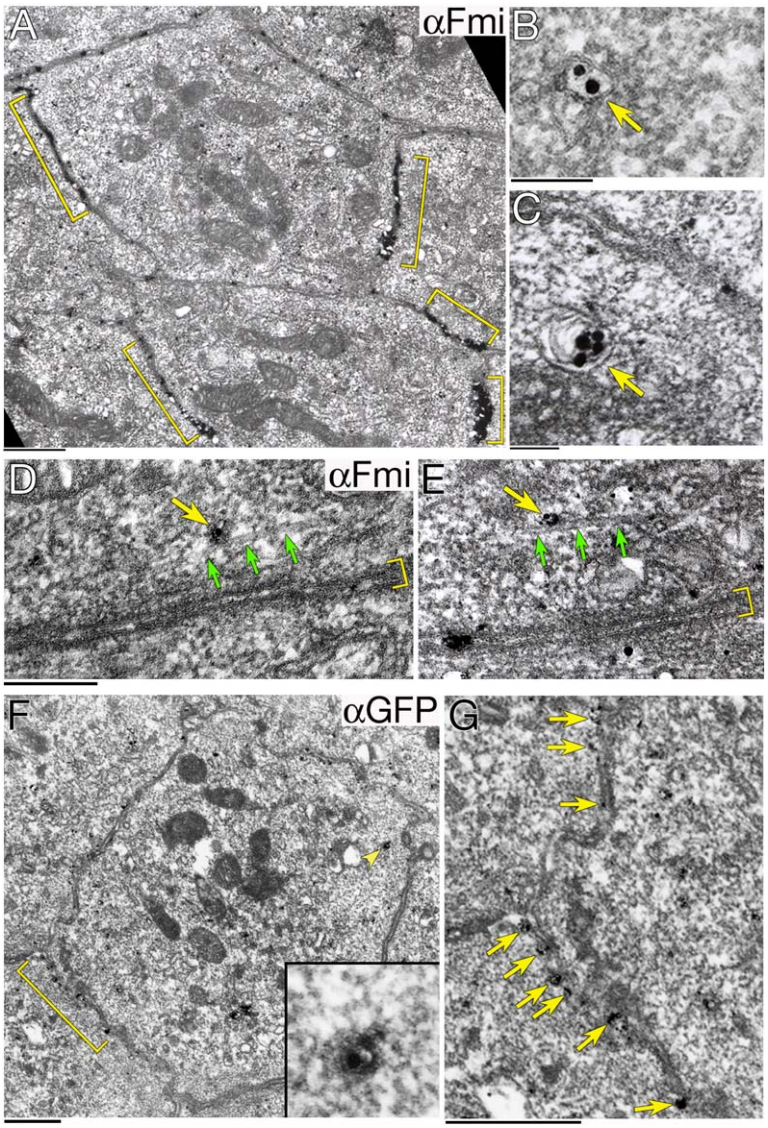

Figure 5. Fmi and Fz::GFP Were Associated with Intracellular Vesicles in Immunoelectron Micrographs

Immuno-EM images of 24 hr APF wings obtained with an Fmi antibody (A–E) and a GFP antibody to detect Fz::GFP (F and G).

(A) Dense signals are seen at P/D cell boundaries (brackets).

(B and C) Signals are localized inside intracellular bilayered vesicles (arrows).

(D and E) Fmi-associated vesicles (yellow arrows) appear to be attached to MTs that are oriented along the P-D axis (green arrows). Brackets indicate intercellular anterior/posterior (A/P) boundaries. The fixation conditions for (D) and (E) were different from those for other panels (see details in the Experimental Procedures).

(F and G) Fz::GFP is closely associated with distal cell boundaries (bracket in [F] and arrows in the close-up view [G]) and with intracellular vesicles (arrowhead and inset in [F]). Genotypes were *yw* (A–E) and *arm-Fz::GFP* (F and G). The scale bars represent 500 nm (A, F, and G), 100 nm (B and C), and 200 nm (D and E).

orientation and length, we defined every longest MT in each cell as a landmark, which appeared to be aligned along the P-D axis, and then addressed how the other MTs in the same cell were oriented with respect to the longest one (Figures S4A and S4B). This analysis strongly suggested that P-D-oriented MTs were predominant in 34 of a total of 42 cells investigated at 24 and 30 hr APF. We also observed P-D-oriented MTs on AJ planes at 18 hr APF (Figures S5A and S5B). Centrioles were often found on the AJ plane, although almost none of the MTs were emanating from those centrioles, and the location of the centriole was not consistent within each interphase or postmitotic wing epidermal cell in terms of the P-D axis (Figures S5C and S5D).

Although imaging individual MTs in wing epidermal cells was technically difficult by light microscopy, our best staining for tubulin showed that filaments, probably bundles of MTs, pointed toward proximal and distal cell boundaries (Figures S6A–S6C) as reported previously (Turner and Adler, 1998). Such P-D-oriented MT bundles were frequently seen at 24 hr APF in live cells that expressed GFP::tubulin, but not at 36 hr APF in cells that had already initiated prehair formation (Figures S6D and S6E). Side-by-side comparison of our EM pictures and light microscopic images strengthened our idea that in the live pupal wing epidermis, individual MTs on the AJ plane were aligned preferentially along the P-D axis before prehair formation.

Fmi and Fz::GFP Are Associated with Intracellular Vesicles in Immunoelectron Micrographs

Based on our time-lapse and conventional EM studies, we favored the idea that Fz::GFP-containing vesicles may be transported distally via the P-D MTs. To test this hypothesis, we visualized Fz::GFP- and Fmi-containing particles in immunoelectron micrographs (Figure 5).

Silver-enhanced Fmi signals were densely localized in extracellular space at P/D cell boundaries, indicating that our pre-embedding protocol worked (brackets in Figure 5A). In addition to these cell boundary signals, we found bilayered vesicles that contained immunogold signals inside (Figures 5B and 5C), and this topological relationship is consistent with the fact that our Fmi antibody recognizes an epitope in the ectodomain of Fmi.

Fifty-four signal-associated vesicles were found in 41 cells observed at 24 hr APF, whereas only four vesicles were labeled with immunogold in 91 cells when a negative control antibody (normal mouse IgG) was used. This result indicates that these intravesicular signals obtained with the Fmi antibody represented endogenous Fmi molecules. We also stained wings that expressed carboxy-terminally GFP-tagged Fz with anti-GFP antibody, and found the immunogold signals to be either closely associated with intracellular surfaces of distal cell boundaries (bracket in Figure 5F and arrows in Figure 5G) or associated with intracellular vesicles (arrowhead and inset in Figure 5F). These Fz::GFP- and Fmi-containing vesicles were present on the AJ plane, strengthening our assumption that these immunogold-positive vesicles corresponded to Fz::GFP particles visualized by confocal microscopy.

Furthermore, we attempted to preserve both MT structures and antibody-antigen binding to examine whether signal-associated vesicles were attached to MTs or not. This was technically a challenging task (see details in the Experimental Procedures); nevertheless, we obtained images where several Fmi signal-containing vesicles appeared to be associated with P-D MTs (Figures 5D and 5E). Taken together, these observations strongly suggest that Fmi and Fz::GFP were contained by intracellular vesicles, and were likely to have been transported to distal cell boundaries along the polarized MT arrays.

To Which Intracellular Compartment Does the Fz::GFP- and Fmi-Containing Vesicle Belong?

Twenty-four hour APF wings expressing Fz::GFP were colabeled with anti-GFP antibody and one of the following compartment marker antibodies: anti-Hrs (endosome marker; Lloyd et al., 2002), anti-KDEL (ER marker; Culi and Mann, 2003), anti-dSyx 16 (Golgi marker; Xu et al., 2002), anti-p120 (Golgi marker; Stanley et al., 1997), or anti-Sec5 (exocyst marker; Murthy et al., 2003). Similarly, *yw* wings of the same age were costained for Fmi and one of the markers. Although punctate signals were detected with any of the above marker antibodies, only a few were colocalized with Fz::GFP or Fmi (data not shown). For example, 7.9% of 189 Fz::GFP particles contained Hrs that is localized in endosomes and regulates endosomal maturation for routing to lysosomes (Lloyd et al., 2002). None of the ER or Golgi markers we tested seemed to be well-colocalized with Fz::GFP or Fmi. In addition to staining fixed wings, we labeled plasma membrane of live cells with a lipophilic dye, FM4-64. This method showed that 32% of the Fz::GFP particles were labeled with FM4-64 (Figure S7), suggesting that a portion of the Fz::GFP particles was endosomes. The remaining particles could have been either endosomes that had been formed before the dye labeling or transport vesicles into which Fz::GFP and Fmi had been loaded in the trans-Golgi network before having been targeted to distal cell boundaries.

Disruption of Microtubules Perturbs Distributions of Fz::GFP and Fmi, and Causes Mislocation of Prehair Formation

To investigate how important the MT network is for normal planar polarization, we disrupted MTs by treating pupae with MT drugs (Figure 6) or by overexpressing KLP10A, MT-depolymerizing kinesin-like protein (Figure S8).

Pupae of 23–24 hr APF were treated with either colchicine or paclitaxel for 6 hr, and then organization of apical MTs and distributions of Fz::GFP and Fmi were observed (Figure 6). The MT network on the AJ plane was disrupted by colchicine treatment in 6 out of 10 wings tested, whereas paclitaxel treatment for the same duration resulted in hyperactive generation and/or bundling of MTs (19%, n = 193; Figures 6A–6C). Fz::GFP distribution was dramatically perturbed in 46 out of 76 live wings and in 6 out of 10 fixed wings that were stained with anti-GFP antibody (Figures 6D–6F), and Fmi localization was similarly affected (Figures 6G–6I). In our time-lapse observations of living cells, Fz::GFP signals at P/D boundaries were reduced and intracellular "blobs" became accumulated over time (Figure 6O). In contrast to the distribution of Fz::GFP and Fmi, that of *D*E-cadherin was not altered under our conditions of the treatment (Figures 6J–6L). This result is consistent with the fact that Fz::GFP particles hardly contained *D*E-cadherin and strongly suggests that under the conditions of our drug treatment, AJ was formed but polarity regulators failed to be localized properly.

About 12–24 hr after the drug treatment, we found that several cells mislocalized F-actin at the centers of cells, a phenocopy of *fz* or *fmi* mutants (4 out of 34; Figures 6M and 6N). In addition to pharmacological approaches, we addressed whether the mislocation phenotype was caused also by expressing KLP10A (Figure S8), which is one of the kinesin-13 family members that do not move along MTs but instead bind to their ends and induce depolymerization (Goshima and Vale, 2005; Mennella et al., 2005). KLP10A expression resulted in moderate decrease in the signal of apical MTs (Figures S8A–S8C), and the mislocation phenotype was observed in 23 out of 62 wings (Figures S8D–S8I).

In addition to the cortical localization, we examined how MT organization and movements of Fz::GFP particles were affected by the colchicine treatment. At 1 hr after the treatment, the MT web was severely disorganized (Movie S8). Whereas more than 70% of the particles moved distally in the control D_1W treatment, directional movements of the particles became less obvious (Figure 6P). The ratio of nondirectionally moving particles significantly increased over time and about 80% of the particles hardly moved in any direction at 6 hr. This result suggested that directional movement of Fz::GFP particles depended on MTs. Taken together, all of these results show that the MT organization contributed to proper distributions of the PCP regulators, specification of the distal cell ends for wing hair formation, and polarized transport of Fz. Conversely, we addressed whether the Fz-mediated signaling itself might be necessary for generation and/or maintenance of the MT array. This did not appear to be the case, as shown by the fact that P-D-oriented MTs were still observed in the absence of Fz function (Figure S9).

Do Noncentrosomal P-D Microtubules Orient Their Plus or Minus Ends toward Distal Cell Boundaries?

A simple explanation for the directional transport of Fz::GFP could be, for example, that most MTs are

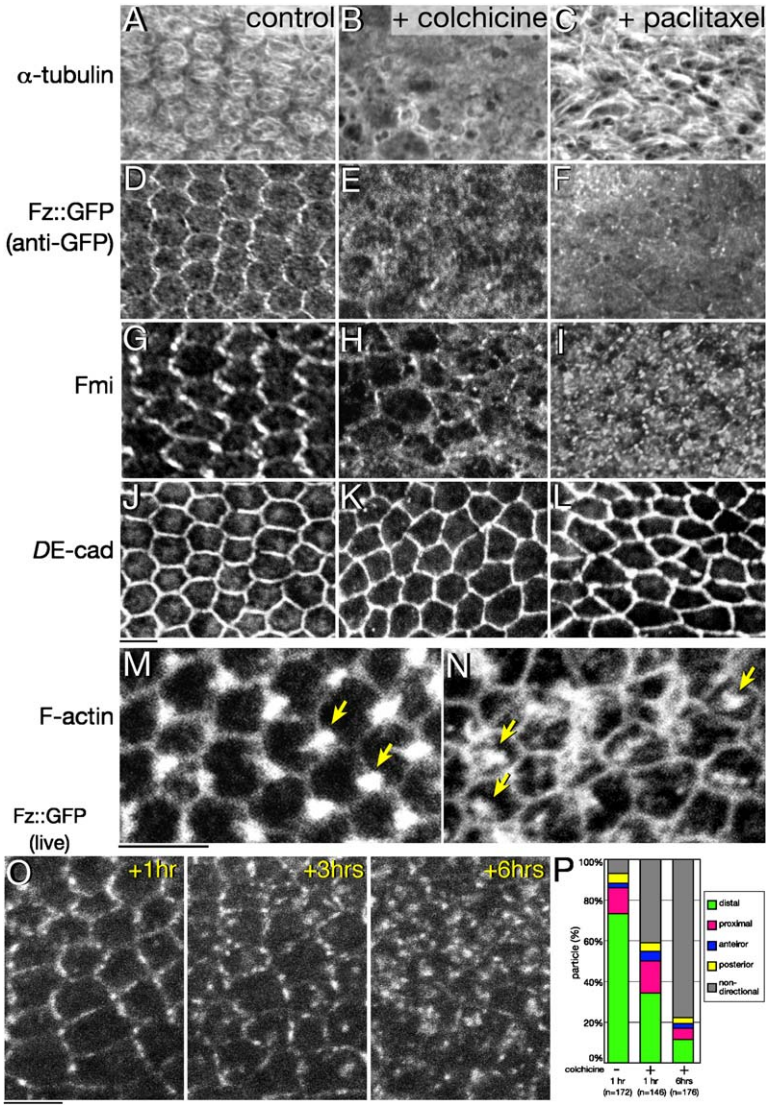

Figure 6. Disruption of Microtubules Perturbs Planar Polarity and the Directional Movement of Fz::GFP Particles

Pupae at 23–24 hr APF were treated with D_1W (control), colchicine, or paclitaxel for 6 hr, fixed, and stained for α-tubulin (A–C), Fz::GFP (D–F), Fmi (G–I), and *D*E-cadherin (J–L). (A, D, and J), (B, E, and K), and (C, F, and L) are images of triple-labeled tissue.

(M and N) Phalloidin staining after 12–24 hr treatment with D_1W (M) or colchicine (N). Prehairs were formed at distal cell edges in the control and at the centers of several colchicine-treated cells (arrows).

(O) Fz::GFP signals in the same live pupae at 1, 3, or 6 hr after colchicine treatment.

(P) Directions of moving particles at 1 or 6 hr after colchicine treatment. Numbers of particles examined were 172 in 43 control wings, 146 in 31 wings at 1 hr, and 176 in 31 wings at 6 hr. The scale bar represents 5 μm.

oriented in the same direction, with their plus ends pointing toward distal boundaries, and that Fz- and Fmi-containing vesicles may be transported by plus (+) end-directed motors. This model is reminiscent of the translocation of Dsh::GFP along the subcortical MT array toward the prospective dorsal side of the *Xenopus* egg (Miller et al., 1999).

To test this possibility, we tracked the dynamic behavior of EB1::GFP in wing cells. EB1 is reported to bind specifically to the ends of growing MTs and is involved in regulation of MT dynamics (Mimori-Kiyosue et al., 2000; Rogers et al., 2002). In 24 hr APF wing cells that expressed EB1::GFP, many comet-like signals with bright fronts and dark tails were shooting (Movies S6–S8), which was very similar to images in EB1::GFP-expressing cells in culture (Mimori-Kiyosue et al., 2000; Rogers et al., 2004). Our observation of wings expressing both EB1::GFP and *D*E-cadherin::GFP showed that those comets were moving on the AJ plane (Figure 7A) at a speed of 0.27 ± 0.054 μm/s (mean ± SD; n = 38, five cells), and this velocity was comparable to the 0.235 μm/s that was reported for *Xenopus* A6 epithelial cells (Mimori-Kiyosue et al., 2000). Importantly, most of these EB1::GFP comets were moving along the P-D axis rather than the A-P axis (Figure 7E), which is consistent with MT orientations (Figures 4A and 4C). This result shows that at least some of the P-D-oriented MTs were dynamic. In each cell, some of the comets were reaching distal cell boundaries and others were moving in the reverse direction (yellow arrows in Figures 7B–7D). Our quantitative analysis shows that distally shooting comets were observed more frequently than proximal-oriented ones with statistical significance (Figure 7F), thus supporting our suspicion that + end-distal MTs were more abundant than + end-proximal MTs.

Discussion

The Polarized Transport Hypothesis and Identity of the Fz::GFP Particle

We propose that Fmi- and Fz::GFP-containing vesicles are transported preferentially toward the distal cell cortex along P-D-oriented MTs (Figure 8). It has been considered that a cassette of transmembrane proteins

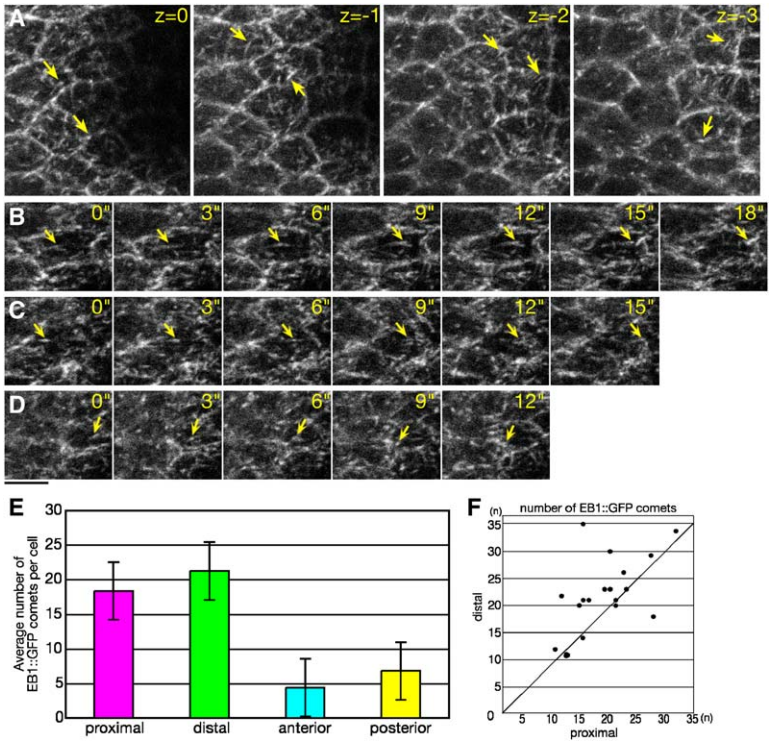

Figure 7. EB1::GFP Comet Assay: There Appears to be a Slight Bias in the P-D Microtubules with More Plus Ends Oriented Distally

(A) Serial Z sections were collected at 1 μm intervals from 0 (apical) to −3 (basal) levels in a 24 hr APF live pupa that coexpressed EB1::GFP and *D*E-cadherin::GFP. Arrows indicate comet-like EB1::GFP signals localized on the AJ plane.

(B–D) A 24 hr APF wing expressing EB1::GFP was imaged at 3 s intervals. Arrows point to examples of "comets." The scale bar represents 5 μm.

(E) Twenty-four hour APF wings were imaged at 2 s intervals for 2 min, the trajectories of 40–83 comet-like signals per cell were classified into their directions, and average numbers of comets of individual classes per cell are shown with standard errors.

(F) The number of proximally shooting comets and that of distally shooting ones in each cell were plotted on x and y axes, respectively, together with a 45° line. Distally shooting comets are more abundant than proximally shooting ones ($p < 0.05$, Wilcoxon test). Numbers of cells examined were 20 in seven wings. Genotypes were *EB1::GFP/+; DE-cadherin::GFP/+* (A) and *EB1::GFP* (B–F).

(Four-jointed, Dachsous, and Fat) functions upstream of Fz and confers an initial small asymmetry of Fz activity across the cell (Lawrence et al., 2004; Ma et al., 2003; Matakatsu and Blair, 2004; Strutt and Strutt, 2002). This small imbalance is amplified through formation of the multiprotein complex across the P/D boundary, reinforces Fz signaling, and eventually leads to specification of prehair formation at the distal cell end (Adler, 2002; Eaton, 2003; Klein and Mlodzik, 2005; Strutt, 2003; Uemura and Shimada, 2003). The polarized transport of Fz we observed may reflect one of the outputs of the upstream cassette to set an initial bias of Fz activity and/or an intermediate step of the Fz signaling feedback amplification (discussed below).

Our immuno-EM studies revealed intracellular vesicles that were associated with Fz::GFP or Fmi on the AJ plane. The number of these vesicles per cell was an order of magnitude higher than that of Fz::GFP particles visualized by confocal microscopy. Only a subpopulation of the vesicles, one containing large numbers of Fz::GFP molecules, may have been detected by our confocal microscopic observations. Although both the multiprotein complex of the cortical PCP signaling components and the *D*E-cadherin-catenin adhesion complex are located at AJ in an almost overlapping manner (Axelrod, 2001; Shimada et al., 2001; Strutt, 2001; Usui et al., 1999), our study supports the possibility that components of these two complexes were separated into distinct vesicles at their exit from the trans-Golgi network (TGN). Sorting of Fz::GFP, Fmi, and possibly Dsh as well from *D*E-cadherin should also take place when molecules on the plasma membrane are incorporated into recycling endosomes. Experiments using mammalian epithelial cell lines have elucidated biosynthetic and recycling pathways for sorting apical and basolateral plasma membrane proteins (Mostov et al., 2003; Rodriguez-Boulan et al., 2005). Wing epidermal cells appear to have a machinery to subdivide molecules that are targeted to AJ.

A Role for the Polarized Transport of Fz and Fmi in the Feedback Amplification and Generation of the Proximal Cortical Domain

Our results of double staining for Fz::GFP and Fmi indicated that the majority of Fmi-containing vesicles were transported distally, not to the proximal boundary. Then how are Fmi, Stbm/Vang, and Pk distributed to the proximal cortex (Figure 1D)?

Fmi, Stbm/Vang, and Pk have already been distributed rather uniformly at the cell cortex in imaginal and early pupal epithelia before the polarized transport starts, and these molecules may be allowed to diffuse laterally within the plasma membrane (Bastock et al., 2003; Tree et al., 2002; Usui et al., 1999). Fmi, which is transported to the distal boundary together with Fz and Dsh, can lock a counterpart on the proximal membrane of the adjacent cell through its homophilic binding property (Usui et al., 1999). Formation of this Fmi-Fmi bridge across the P/D boundary would anchor the Fz-Dsh complex at the distal cortex, increasing local activity and the copy number of Fz-Dsh (Figure 8A). This slight input may initiate recruitment of Stbm/Vang-Pk on the opposing proximal cortex by means of mutual exclusion between Dsh and Pk, and by means of hypothetical ectodomain interaction between Fz and Stbm/Vang (Amonlirdviman et al., 2005; Eaton, 2003; Klein and Mlodzik, 2005; Strutt, 2003). Then the nascent asymmetric complex amplifies the imbalance of Fz activity by unknown mechanisms. This amplification could be involved in either facilitating loading Fz-Dsh and Fmi into vesicles at their exit from the TGN, accelerating the transport of the vesicles to the distal cortex, and/or

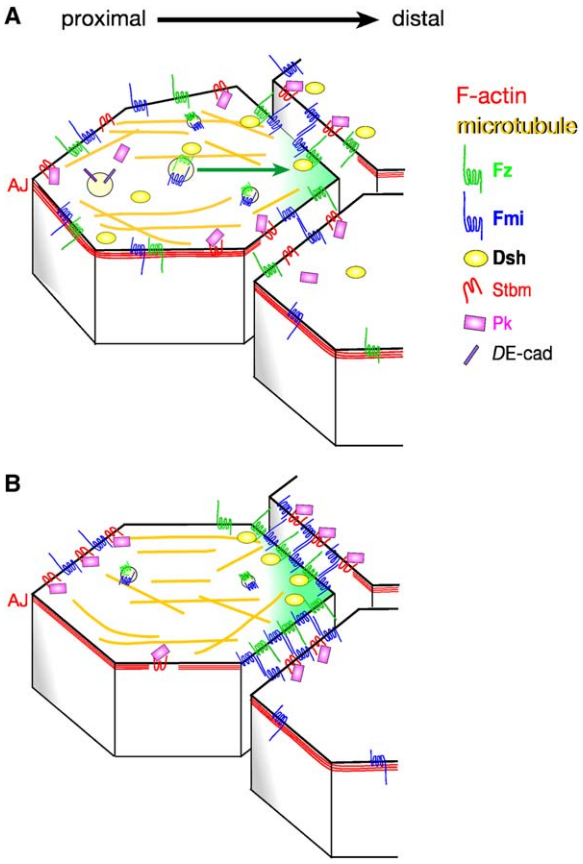

Figure 8. Models of the Polarized Transport of Fz-Dsh and Fmi along P-D-Oriented Microtubules

Preferential transport toward distal cell boundaries for several hours before prehair formation (A) is hypothesized to lead to establishment of cortical domains just before the onset of prehair formation (B). See details in the text. Cell geometry is more irregular at earlier stages and this is reflected in the diagram (A).

restricting diffusion of Fz-Dsh and Stbm/Vang-Pk out of the distal and proximal membrane domains, respectively (Figure 8B).

In setting up the initial bias, the polarized transport may not necessarily require Stbm and Pk, whereas the subsequent amplification presumably depends on the formation of the cortical complex. This hypothesis is consistent with our observation that bright Fz::GFP particles were hardly seen in the *dsh*, *fmi*, or *pk* mutant backgrounds. It also explains why Fz^{P278L}::YFP particles did not move distally, because Fz^{P278L} is postulated to lose its interaction with Dsh (Amonlirdviman et al., 2005; Axelrod, 2001) and most Fz^{P278L}::YFP particles did not contain Fmi.

Most Likely P-D-Oriented MTs on the AJ Plane Contribute to the Cortical Distribution of the PCP Regulators

Besides noncentrosomal MTs along the apicobasal axis (Mogensen et al., 1989), we unequivocally visualized P-D-oriented MTs in the AJ plane and showed the important role of this MT array in localizing the cortical PCP proteins and the distal-oriented movement of Fz::GFP particles. Assuming the importance of the P-D MT alignment, how is the Fz::GFP particle transported or recycled back along the MT track in terms of vesicular trafficking? The particles showed staggered trajectories when followed at 1 or 10 s intervals, and this back-and-forth motion of the Fz::GFP particle can be interpreted as follows: (1) individual Fz::GFP particles bind multiple motors of different classes, and (2) activities of the motors of opposing directionality are coordinated. This bidirectional transport has been shown for organelle trafficking; despite such back-and-forth motion, cargos can still achieve net transport on longer time scales (Hirokawa, 1998; Kural et al., 2005; Welte, 2004). Another, not mutually exclusive, possibility could be that the particle/cargo motor complex may repeat cycles of running, falling off the MT track, and reengaging. Whether specific members of MT motors contribute to the Fz::GFP transport or not awaits further genetic as well as biochemical characterization of the particle.

Given that either of the above possibilities of motor-driven motions is the case, why did the Fz::GFP particle move predominantly toward distal cell boundaries when followed at 1 min intervals? We attempted to trace the origin of this asymmetry to the polarity of individual P-D MTs and found that the wing cell had slightly more + end-distal MTs than + end-proximal ones. Nevertheless, it is an open question as to whether such a small difference can be causally related to the distally oriented transport and whether the subtle difference in MT polarity can be one of the critical parameters in operating the cortical feedback loop.

How Are Noncentrosomal MTs Aligned Approximately along the P-D Axis at the Level of Adherens Junction?

P-D-oriented MTs were still observed in the absence of Fz function, and this strongly suggests that generation of the P-D MT array is controlled by a mechanism upstream of, or separate from, the cortical complex. One clue for this mechanism involving MTs may be Widerborst (Wdb), a B′ regulatory subunit of PP2A (Eaton, 2003; Hannus et al., 2002). It would be necessary to investigate how exactly MTs are disorganized when Wdb function is abrogated. Another clue may be a recent report that the presence of apical MTs is related to Dpp signaling activity, although a cytoskeletal function for Dpp remains to be shown (Gibson and Perrimon, 2005; Shen and Dahmann, 2005).

A large gap remains in our cell biological understanding of the global cue that is considered to be provided by the cassette of transmembrane proteins (Fj, Ds, and Ft; Ma et al., 2003; Matakatsu and Blair, 2004; Simon, 2004; Strutt and Strutt, 2002; Yang et al., 2002). It should be pointed out that each of Fj, Ds, and Ft controls the ratio of proximal-distal to anterior-posterior growth of appendages (Mohr, 1923; Stern and Bridges, 1927; Waddington, 1940, 1943) and that Ds and Ft have been recently shown to control the shape of the growing organs by regulating orientations of cell divisions in imaginal discs (Baena-Lopez et al., 2005). This supports the hypothesis that Ds and Ft can orient the mitotic spindle, and hence MT organization, during wing morphogenesis. It would be intriguing to investigate whether the MT orientation and polarity observed in this study are also under the control of the upstream cassette, and to

pursue a molecular connection between tissue shape and polarity.

Experimental Procedures

Fly Stocks

Control, transgenic, or mutant strains used were *yw*, *arm-Fz::GFP*, *Act-Fz^{P278L}::YFP* (Strutt, 2001), *ubi-DEcadherin::GFP* (Oda and Tsukita, 2001), *dsh^{1}* (Theisen et al., 1994), *fz^{K21}*, *Df(3L)fz^{D21}* (Jones et al., 1996), and *pk$^{pk\text{-}sple13}$* (Gubb et al., 1999). Several transgenes were expressed by using the GAL4/UAS system (Brand and Perrimon, 1993). UAS strains were *UAS-fmi dsRNA* (K. Sugimura, M. Yamamoto, and T.U., unpublished results), *UAS-GFP::actin* (Verkhusha et al., 1999), *UAS-GFP::tubulin* (Grieder et al., 2000), *UAS-KLP10A*, *UAS-KLP10A::GFP*, and driver strains were *patched* (*ptc*)-*GAL4*, *engrailed* (*en*)-GAL4, and *daughterless* (*da*)-*GAL4*. cDNA clones of *KLP10A* and *KLP10A::GFP* were gifts from G. Goshima. EB1::GFP was created by fusing enhanced GFP to the C-terminal end of *Drosophila* EB1 under the ubiquitin promoter (Elliott et al., 2005; Lee et al., 1988), and this EB1::GFP mimics the behavior of endogenous EB1 including microtubule + end tracking (H.O., unpublished results).

Immunohistochemistry

Reagents used were anti-Fmi mAb (#74; Usui et al., 1999), anti-GFP rabbit serum (Molecular Probes, Eugene, OR), DCAD2 (Oda et al., 1994), anti-tubulin mAb (Seikagaku, Tokyo, Japan or Sigma, St. Louis, MO), anti-Dsh (Shimada et al., 2001), and phalloidin-Alexa (Molecular Probes). Tubulin staining was performed as previously described (Rogers et al., 2002).

Time-Lapse Observation of Living Pupal Wing Cells

A small piece of a pupal case was removed and the pupa was placed on a glass-bottomed dish. GFP signals were imaged with a laser scanning confocal microscope. See details in the legend of Figure S1B. This protocol enabled us to image cells in the central region of B-D (Figure 1A). In our drug treatment experiments, pupae were soaked in distilled water containing 1 mg/ml colchicine (Sigma) or in dimethyl sulfoxide containing 50–500 μM paclitaxel (Alexis, Lausen, Switzerland). To label cell membranes with the lipophilic dye FM4-64 (Molecular Probes), we used a Femtotips II needle (Eppendorf, Hamburg, Germany) to put a drop of 150 μM solution on the surface of the wing cuticle.

Electron Microscopy

Details of procedures for conventional electron microscopy and pre-embedding immunoelectron microscopy are described in Supplemental Data. To define the proximal-distal (P-D) orientation of each wing on each ultrathin section, we embedded a 24–30 hr APF wing and a 36 hr APF wing side by side, and used the sensory bristles of the anterior wing margin of the 36 hr APF wing for landmarks of the P-D orientation. Length and angles of MTs were measured in image files by using ImageJ (http://rsb.info.nih.gov/ij/). For pre-embedding immunoelectron microscopy, dissected pupae were fixed in either of two fixatives: periodate-lysine-paraformaldehyde (PLP) fixative or a mixture of paraformaldehyde (PFA) and glutaraldehyde (GA) in PBS. Wings were fixed in the mixture of PFA and GA only when we attempted to preserve both MTs and the antibody binding (Figures 5D and 5E). Due to this compromise between the two requirements, signal-containing vesicles were found in much fewer cells compared to those in cells that were fixed by PLP (Figures 5A–5C), and both length and number of MTs observed were substantially reduced compared to those in Figures 3 and 4.

Supplemental Data

Supplemental Data include Experimental Procedures, nine figures, and eight movies, and are available at http://www.developmentalcell.com/cgi/content/full/10/2/209/DC1/.

Acknowledgments

We thank M. Takeichi, S. Hayashi, and members of S. Yonemura's lab for allowing Y.S. to perform EM studies at the Center for Developmental Biology, RIKEN. We are also grateful to P. Adler, J. Axelrod, A. Spradling, H. Oda, S. Goto, G. Goshima, the Berkeley *Drosophila* Genome Project, the Bloomington Stock Center, and the *Drosophila* Genetic Resource Center of the Kyoto Institute of Technology for reagents, and K. Sugimura and M. Yamamoto for fly strains. We thank very much H. Otsuna, K. Ito, F. Kano, M. Murata, H. Akimaru, H. Shimizu, M. Mishima, K. Kinoshita, and R. Niwa for technical advice and encouragement, and Shoichiro Tsukita and Sachiko Tsukita for use of their electron microscope at the final stage of this study. This work was supported by grants to T.U. from JST/CREST and from the Toray Foundation (Japan) for the Promotion of Science. H.O. and D.S. are recipients of senior research fellowships from the Welcome Trust. Y.S. is a recipient of a Fellowship of the Japan Society for the Promotion of Science for Junior Scientists.

Received: August 25, 2005
Revised: November 5, 2005
Accepted: November 21, 2005
Published: February 6, 2006

References

Adler, P.N. (2002). Planar signaling and morphogenesis in *Drosophila*. Dev. Cell *2*, 525–535.

Amonlirdviman, K., Khare, N.A., Tree, D.R., Chen, W.S., Axelrod, J.D., and Tomlin, C.J. (2005). Mathematical modeling of planar cell polarity to understand domineering nonautonomy. Science *307*, 423–426.

Axelrod, J.D. (2001). Unipolar membrane association of Dishevelled mediates Frizzled planar cell polarity signaling. Genes Dev. *15*, 1182–1187.

Baena-Lopez, L.A., Baonza, A., and Garcia-Bellido, A. (2005). The orientation of cell divisions determines the shape of *Drosophila* organs. Curr. Biol. *15*, 1640–1644.

Bastock, R., Strutt, H., and Strutt, D. (2003). Strabismus is asymmetrically localised and binds to Prickle and Dishevelled during *Drosophila* planar polarity patterning. Development *130*, 3007–3014.

Brand, A.H., and Perrimon, N. (1993). Targeted gene expression as a means of altering cell fates and generating dominant phenotypes. Development *118*, 401–415.

Chae, J., Kim, M.J., Goo, J.H., Collier, S., Gubb, D., Charlton, J., Adler, P.N., and Park, W.J. (1999). The *Drosophila* tissue polarity gene starry night encodes a member of the protocadherin family. Development *126*, 5421–5429.

Culi, J., and Mann, R.S. (2003). Boca, an endoplasmic reticulum protein required for wingless signaling and trafficking of LDL receptor family members in *Drosophila*. Cell *112*, 343–354.

Curtin, J.A., Quint, E., Tsipouri, V., Arkell, R.M., Cattanach, B., Copp, A.J., Henderson, D.J., Spurr, N., Stanier, P., Fisher, E.M., et al. (2003). Mutation of Celsr1 disrupts planar polarity of inner ear hair cells and causes severe neural tube defects in the mouse. Curr. Biol. *13*, 1129–1133.

Davies, A., Formstone, C., Mason, I., and Lewis, J. (2005). Planar polarity of hair cells in the chick inner ear is correlated with polarized distribution of c-flamingo-1 protein. Dev. Dyn. *233*, 998–1005.

Drubin, D., ed. (2000). Cell Polarity (New York: Oxford University Press).

Eaton, S. (2003). Cell biology of planar polarity transmission in the *Drosophila* wing. Mech. Dev. *120*, 1257–1264.

Eaton, S., Wepf, R., and Simons, K. (1996). Roles for Rac1 and Cdc42 in planar polarization and hair outgrowth in the wing of *Drosophila*. J. Cell Biol. *135*, 1277–1289.

Elliott, S.L., Cullen, C.F., Wrobel, N., Kernan, M.J., and Ohkura, H. (2005). EB1 is essential during *Drosophila* development and plays a crucial role in the integrity of chordotonal mechanosensory organs. Mol. Biol. Cell *16*, 891–901.

Feiguin, F., Hannus, M., Mlodzik, M., and Eaton, S. (2001). The ankyrin repeat protein Diego mediates Frizzled-dependent planar polarization. Dev. Cell *1*, 93–101.

Fristrom, D., and Fristrom, J.W. (1975). The mechanisms of evagination of imaginal discs of *Drosophila melanogaster*. I. General considerations. Dev. Biol. *43*, 1–23.

Gibson, M.C., and Perrimon, N. (2005). Extrusion and death of DPP/BMP-compromised epithelial cells in the developing *Drosophila* wing. Science *307*, 1785–1789.

Goshima, G., and Vale, R.D. (2005). Cell cycle-dependent dynamics and regulation of mitotic kinesins in *Drosophila* S2 cells. Mol. Biol. Cell *16*, 3896–3907.

Grieder, N.C., de Cuevas, M., and Spradling, A.C. (2000). The fusome organizes the microtubule network during oocyte differentiation in *Drosophila*. Development *127*, 4253–4264.

Gubb, D., Green, C., Huen, D., Coulson, D., Johnson, G., Tree, D., Collier, S., and Roote, J. (1999). The balance between isoforms of the prickle LIM domain protein is critical for planar polarity in *Drosophila* imaginal discs. Genes Dev. *13*, 2315–2327.

Hannus, M., Feiguin, F., Heisenberg, C.P., and Eaton, S. (2002). Planar cell polarization requires Widerborst, a B' regulatory subunit of protein phosphatase 2A. Development *129*, 3493–3503.

Hirokawa, N. (1998). Kinesin and dynein superfamily proteins and the mechanism of organelle transport. Science *279*, 519–526.

Jones, K.H., Liu, J., and Adler, P.N. (1996). Molecular analysis of EMS-induced frizzled mutations in *Drosophila melanogaster*. Genetics *142*, 205–215.

Katanaev, V.L., Ponzielli, R., Semeriva, M., and Tomlinson, A. (2005). Trimeric G protein-dependent frizzled signaling in *Drosophila*. Cell *120*, 111–122.

Klein, T.J., and Mlodzik, M. (2005). Planar cell polarization: an emerging model points in the right direction. Annu. Rev. Cell Dev. Biol. *21*, 155–176.

Klingensmith, J., Nusse, R., and Perrimon, N. (1994). The *Drosophila* segment polarity gene dishevelled encodes a novel protein required for response to the wingless signal. Genes Dev. *8*, 118–130.

Kural, C., Kim, H., Syed, S., Goshima, G., Gelfand, V.I., and Selvin, P.R. (2005). Kinesin and dynein move a peroxisome in vivo: a tug-of-war or coordinated movement? Science *308*, 1469–1472.

Lawrence, P.A. (1966). Gradients in the insect segment: the orientation of hairs in the milkweed bug *Oncopeltus fasciatus*. J. Exp. Biol. *44*, 607–620.

Lawrence, P.A., Casal, J., and Struhl, G. (2004). Cell interactions and planar polarity in the abdominal epidermis of *Drosophila*. Development *131*, 4651–4664.

Lee, H.S., Simon, J.A., and Lis, J.T. (1988). Structure and expression of ubiquitin genes of *Drosophila melanogaster*. Mol. Cell. Biol. *8*, 4727–4735.

Lloyd, T.E., Atkinson, R., Wu, M.N., Zhou, Y., Pennetta, G., and Bellen, H.J. (2002). Hrs regulates endosome membrane invagination and tyrosine kinase receptor signaling in *Drosophila*. Cell *108*, 261–269.

Ma, D., Yang, C.H., McNeill, H., Simon, M.A., and Axelrod, J.D. (2003). Fidelity in planar cell polarity signalling. Nature *421*, 543–547.

Matakatsu, H., and Blair, S.S. (2004). Interactions between Fat and Dachsous and the regulation of planar cell polarity in the *Drosophila* wing. Development *131*, 3785–3794.

Mennella, V., Rogers, G.C., Rogers, S.L., Buster, D.W., Vale, R.D., and Sharp, D.J. (2005). Functionally distinct kinesin-13 family members cooperate to regulate microtubule dynamics during interphase. Nat. Cell Biol. *7*, 235–245.

Miller, J.R., Rowning, B.A., Larabell, C.A., Yang-Snyder, J.A., Bates, R.L., and Moon, R.T. (1999). Establishment of the dorsal-ventral axis in *Xenopus* embryos coincides with the dorsal enrichment of dishevelled that is dependent on cortical rotation. J. Cell Biol. *146*, 427–437.

Mimori-Kiyosue, Y., Shiina, N., and Tsukita, S. (2000). The dynamic behavior of the APC-binding protein EB1 on the distal ends of microtubules. Curr. Biol. *10*, 865–868.

Mlodzik, M. (2002). Planar cell polarization: do the same mechanisms regulate *Drosophila* tissue polarity and vertebrate gastrulation? Trends Genet. *18*, 564–571.

Mogensen, M.M., Tucker, J.B., and Stebbings, H. (1989). Microtubule polarities indicate that nucleation and capture of microtubules occurs at cell surfaces in *Drosophila*. J. Cell Biol. *108*, 1445–1452.

Mohr, O.L. (1923). Modifications of the sex-ratio through a sex-linked semi-lethal in *Drosophila melanogaster*. (Besides notes on an autosomal section deficiency.). Studia Mendeliana (Brunn) 266–287.

Mostov, K., Su, T., and ter Beest, M. (2003). Polarized epithelial membrane traffic: conservation and plasticity. Nat. Cell Biol. *5*, 287–293.

Murthy, M., Garza, D., Scheller, R.H., and Schwarz, T.L. (2003). Mutations in the exocyst component Sec5 disrupt neuronal membrane traffic, but neurotransmitter release persists. Neuron *37*, 433–447.

Oda, H., and Tsukita, S. (2001). Real-time imaging of cell-cell adherens junctions reveals that *Drosophila* mesoderm invagination begins with two phases of apical constriction of cells. J. Cell Sci. *114*, 493–501.

Oda, H., Uemura, T., Harada, Y., Iwai, Y., and Takeichi, M. (1994). A *Drosophila* homolog of cadherin associated with armadillo and essential for embryonic cell-cell adhesion. Dev. Biol. *165*, 716–726.

Rodriguez-Boulan, E., Kreitzer, G., and Musch, A. (2005). Organization of vesicular trafficking in epithelia. Nat. Rev. Mol. Cell Biol. *6*, 233–247.

Rogers, S.L., Rogers, G.C., Sharp, D.J., and Vale, R.D. (2002). *Drosophila* EB1 is important for proper assembly, dynamics, and positioning of the mitotic spindle. J. Cell Biol. *158*, 873–884.

Rogers, S.L., Wiedemann, U., Hacker, U., Turck, C., and Vale, R.D. (2004). *Drosophila* RhoGEF2 associates with microtubule plus ends in an EB1-dependent manner. Curr. Biol. *14*, 1827–1833.

Shen, J., and Dahmann, C. (2005). Extrusion of cells with inappropriate Dpp signaling from *Drosophila* wing disc epithelia. Science *307*, 1789–1790.

Shimada, Y., Usui, T., Yanagawa, S., Takeichi, M., and Uemura, T. (2001). Asymmetric colocalization of Flamingo, a seven-pass transmembrane cadherin, and Dishevelled in planar cell polarization. Curr. Biol. *11*, 859–863.

Simon, M.A. (2004). Planar cell polarity in the *Drosophila* eye is directed by graded Four-jointed and Dachsous expression. Development *131*, 6175–6184.

Stanley, H., Botas, J., and Malhotra, V. (1997). The mechanism of Golgi segregation during mitosis is cell type-specific. Proc. Natl. Acad. Sci. USA *94*, 14467–14470.

Stern, C., and Bridges, C.B. (1927). The mutants of the extreme left end of the second chromosome of *Drosophila melanogaster*. Genetics *11*, 503–530.

Strutt, D.I. (2001). Asymmetric localization of frizzled and the establishment of cell polarity in the *Drosophila* wing. Mol. Cell *7*, 367–375.

Strutt, D.I. (2002). The asymmetric subcellular localisation of components of the planar polarity pathway. Semin. Cell Dev. Biol. *13*, 225–231.

Strutt, D. (2003). Frizzled signalling and cell polarisation in *Drosophila* and vertebrates. Development *130*, 4501–4513.

Strutt, H., and Strutt, D. (2002). Nonautonomous planar polarity patterning in *Drosophila*: dishevelled-independent functions of frizzled. Dev. Cell *3*, 851–863.

Theisen, H., Purcell, J., Bennett, M., Kansagara, D., Syed, A., and Marsh, J.L. (1994). dishevelled is required during wingless signaling to establish both cell polarity and cell identity. Development *120*, 347–360.

Torban, E., Kor, C., and Gros, P. (2004). Van Gogh-like2 (Strabismus) and its role in planar cell polarity and convergent extension in vertebrates. Trends Genet. *20*, 570–577.

Tree, D.R., Shulman, J.M., Rousset, R., Scott, M.P., Gubb, D., and Axelrod, J.D. (2002). Prickle mediates feedback amplification to generate asymmetric planar cell polarity signaling. Cell *109*, 371–381.

Turner, C.M., and Adler, P.N. (1998). Distinct roles for the actin and microtubule cytoskeletons in the morphogenesis of epidermal hairs during wing development in *Drosophila*. Mech. Dev. *70*, 181–192.

Uemura, T., and Shimada, Y. (2003). Breaking cellular symmetry along planar axes in *Drosophila* and vertebrates. J. Biochem. (Tokyo) *134*, 625–630.

Usui, T., Shima, Y., Shimada, Y., Hirano, S., Burgess, R.W., Schwarz, T.L., Takeichi, M., and Uemura, T. (1999). Flamingo, a seven-pass transmembrane cadherin, regulates planar cell polarity under the control of Frizzled. Cell *98*, 585–595.

Veeman, M.T., Axelrod, J.D., and Moon, R.T. (2003). A second canon. Functions and mechanisms of β-catenin-independent Wnt signaling. Dev. Cell *5*, 367–377.

Verkhusha, V.V., Tsukita, S., and Oda, H. (1999). Actin dynamics in lamellipodia of migrating border cells in the *Drosophila* ovary revealed by a GFP-actin fusion protein. FEBS Lett. *445*, 395–401.

Vinson, C.R., Conover, S., and Adler, P.N. (1989). A *Drosophila* tissue polarity locus encodes a protein containing seven potential transmembrane domains. Nature *338*, 263–264.

Waddington, C.H. (1940). The genetic control of wing development in *Drosophila*. J. Genet. *41*, 75–139.

Waddington, C.H. (1943). The development of some 'leg genes' in *Drosophila*. J. Genet. *45*, 39–43.

Welte, M.A. (2004). Bidirectional transport along microtubules. Curr. Biol. *14*, R525–R537.

Wong, L.L., and Adler, P.N. (1993). Tissue polarity genes of *Drosophila* regulate the subcellular location for prehair initiation in pupal wing cells. J. Cell Biol. *123*, 209–221.

Xu, H., Boulianne, G.L., and Trimble, W.S. (2002). *Drosophila* syntaxin 16 is a Q-SNARE implicated in Golgi dynamics. J. Cell Sci. *115*, 4447–4455.

Yang, C.H., Axelrod, J.D., and Simon, M.A. (2002). Regulation of Frizzled by fat-like cadherins during planar polarity signaling in the *Drosophila* compound eye. Cell *108*, 675–688.